ADVANCED MATERIALS
www.advmat.de

Check for updates

Triboiontronic Transistor of MoS_2

Guoyun Gao, Jinran Yu, Xixi Yang, Yaokun Pang, Jing Zhao, Caofeng Pan, Qijun Sun, and Zhong Lin Wang**

Electric double layers (EDLs) formed in electrolyte-gated field-effect transistors (FETs) induce an extremely large local electric field that gives a highly efficient charge carrier control in the semiconductor channel. To achieve highly efficient triboelectric potential gating on the FET and explore diversified applications of electric double layer FETs (EDL-FETs), a triboiontronic transistor is proposed to bridge triboelectric potential modulation and ion-controlled semiconductor devices. Utilizing the triboelectric potential instead of applying an external gate voltage, the triboiontronic MoS_2 transistor is efficiently operated owing to the formation of EDLs in the ion-gel dielectric layer. The operation mechanism of the triboiontronic transistor is proposed, and high current on/off ratio over 10^7, low threshold value (75 µm), and steep switching properties (20 µm dec^{-1}) are achieved. A triboiontronic logic inverter with desirable gain (8.3 V mm^{-1}), low power consumption, and high stability is also demonstrated. This work presents a low-power-consuming, active, and a general approach to efficiently modulate semiconductor devices through mechanical instructions, which has great potential in human–machine interaction, electronic skin, and intelligent wearable devices. The proposed triboiontronics utilize ion migration and arrangement triggered by mechanical stimuli to control electronic properties, which are ready to deliver new interdisciplinary research directions.

The electrostatic charges originated from contact electrification (triboelectrification) between two different materials create an electrical field to drive free electrons to flow through external circuit (e.g., resistor-type electrical appliance), inducing pulse output signals. The triboelectric nanogenerators (TENGs) utilize the pulse outputs to fulfill mechanical energy conversion into electricity, gaining great achievement in energy harvesting via various mechanical movements,[1,2] self-powered mechanosensations (or systems),[3–6] highly sensitive mass spectrometric analysis,[7] mechanical-triggered plasma in atmospheric pressure,[8] etc.[9,10] When the TENG-derived electrostatic field is coupled with capacitive devices (e.g., field effect transistors, FETs), field effect of triboelectric potential instead of pulse output is imposed to modulate the channel Fermi level and transport properties. The coupling between triboelectric potential and semiconductor devices leads to a new field of tribotronics,[11–13] involving electromechanical modulation in logic devices,[14] tactile sensors,[15,16] phototransistors,[17] memory,[18] etc. To exploit adaptive and high-performance tribotronic devices, both fundamental research and technical engineering on TENG, corresponding semiconductor devices, and their coupling characteristics are urgent to be implemented. Dual-gate capacitive coupling enables tribotronic MoS_2 transistor to achieve a high current on/off ratio at $\approx 10^6$.[14] Planar design and utilization of direct-contact mode also greatly simplifies graphene tribotronic mechanosensation.[19] However, there is still large space to make progress on tribotronics engineering due to the previous complex fabrication process and relatively poor performance.

For a typical FET, it is desirable to have a high capacitance gate dielectric to induce ultrahigh electric field to accumulate more charge carries. The electrolyte gating under an electric field creates prompt and strong accumulation of ions and

G. Gao, J. Yu, X. Yang, Dr. Y. Pang, Dr. J. Zhao, Prof. C. Pan, Prof. Q. Sun, Prof. Z. L. Wang
Beijing Institute of Nanoenergy and Nanosystems
Chinese Academy of Sciences
Beijing 100083, P. R. China
E-mail: sunqijun@binn.cas.cn; zhong.wang@mse.gatech.edu

G. Gao, J. Yu, X. Yang, Dr. Y. Pang, Dr. J. Zhao, Prof. C. Pan, Prof. Q. Sun, Prof. Z. L. Wang
School of Nanoscience and Technology
University of Chinese Academy of Sciences
Beijing 100049, P. R. China

Prof. C. Pan, Prof. Q. Sun, Prof. Z. L. Wang
Center on Nanoenergy Research
School of Physical Science and Technology
Guangxi University
Nanning 530004, China

Prof. Z. L. Wang
School of Materials Science and Engineering
Georgia Institute of Technology
Atlanta, GA 30332-0245, USA

The ORCID identification number(s) for the author(s) of this article can be found under https://doi.org/10.1002/adma.201806905.

DOI: 10.1002/adma.201806905

 © 2018 WILEY-VCH Verlag GmbH & Co. KGaA, Weinheim

compensated charge carries at the interface of electrolyte/semiconductor, inducing an electric double layer (EDL).[20–22] The EDL is considered as a nanogap capacitor bearing nearly all the external gate voltage drop, which can cause an extremely large electric field to efficiently control the charge carrier density in semiconductor channel.[23–25] The EDL–FET method is promising for low-power consumption transistors,[26,27] printable electronic devices,[20] fundamental physics research,[28–30] bio/chemical sensors,[31] and artificial synapse.[32–34] Moreover, EDL represents an interaction between ions and electrons, deriving an interdisciplinary research direction to controlling electronic properties through ions migration/transport and rearrangement, i.e., ion-controlled electronics.[24] Through highly efficient EDL modulation, even unusual 2D superconductivity and magnetic anisotropy interaction based on phase transitions are demonstrated.[28,30] Recently, 2D transition-metal dichalcogenides (2D-TMDs) have been extensively investigated for next generation semiconductor devices.[35,36] Atomically thin MoS_2 has been widely explored as a highly promising channel material for 2D-materials-based FETs due to its ideal electrostatic control of the channel, ambient stability, an appropriate direct bandgap and the moderate mobility.[37,38] In the future era of the Internet of Things (IoTs), how to take advantage of ions migrations triggered by mechanical motions to tune unprecedented electrical behaviors is greatly demanded.

Here, we proposed a triboiontronic FET of molybdenum disulfide (MoS_2) to bridge triboelectric potential modulation and ion-controlled semiconductor devices. The triboelectric potential produced from TENG was coupled with an electrolyte-gated MoS_2 FET. The EDLs with ultrahigh capacitance were induced at the interface between the ion gel and the semiconductor upon the triboelectric potential, which enabled highly efficient charge carrier control in the semiconductor channel. Without applying gate voltage, triboiontronic MoS_2 transistor was efficiently operated in active mode with low threshold value at 75 µm and steep switch properties of 20 µm dec^{-1}. Through presetting the initial triboelectric potential coupled to the transistor, triboiontronic transistor was able to operate in both depletion/enhancement mode (D-/E-mode) with high current on/off ratio exceeding 10^7 and ultralow cutoff current below 0.1 pA. The operation mechanism of high performance triboiontronic transistor was explained in details correlating triboelectric potential coupling with EDLs formation. The encapsulation of the source–drain electrodes and solidification of ion-gel gate dielectric was essential for the highly stable and durable electrical properties. The triboiontronic logic inverter with a desirable voltage gain of (8.3 V mm^{-1}), low power consumption and high stability was also demonstrated. This work presents a low-power-consuming, active, and a general approach to efficiently modulate semiconductor devices and logic circuits based on 2D materials through external instructions, which have great potential in human–machine interaction, electronic skin, intelligent sensor, and other wearable devices.

The tribotronic FET is a device that uses triboelectric potential to control the electronic transport behavior. For ion-gel-gated tribotronic FET (i.e., triboiontronic FET), triboelectric potential derived EDL enables more efficient charge carrier control in the semiconductor channel due to the induced ultrahigh electric fields at the interface. Prior to investigating the electric performance of the triboiontronic transistor, the EDLs formation process induced by the triboelectric potential was first proposed. **Figure 1**a schematically shows the ions migration process in the ion gel with a parallel-plate capacitor model (metal/ion-gel/metal structure) to illustrate the equivalent MIS (gate–insulator–semiconductor) gating mechanism. The ion gel is intrinsically an ion liquid (1-ethyl-3-methylimidazolium bis(trifluoromethylsulfonyl)imide ([EMIM][TFSI]) gelation in a photo-crosslinked polymer network. The TENG is composed

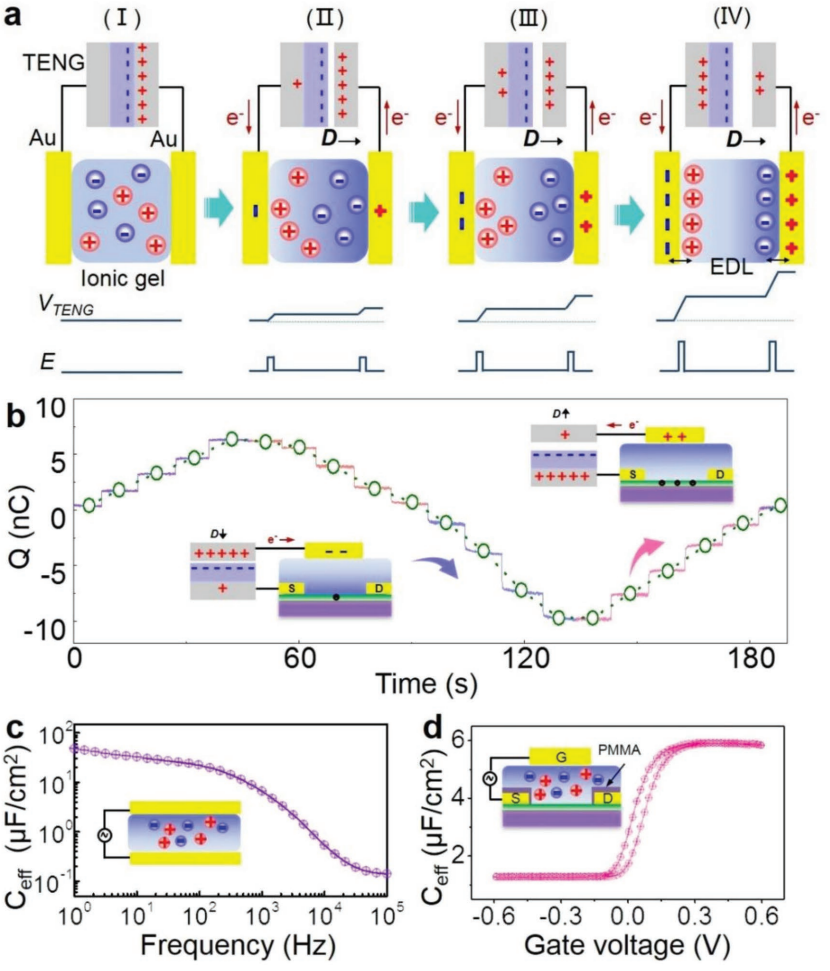

Figure 1. a) Schematic illustrations of the T-EDLs formation process and corresponding charge distributions. Bottom panels are the triboelectric potential V_{TENG} and electric field E in the ion gel at each state. b) The quantity of transferred charges in one separation–contact–separation cycle. c) Specific capacitance of MIM capacitor versus the applied frequency. d) Specific capacitance of MoS_2 FET capacitor versus the applied gate voltage.

© 2018 WILEY-VCH Verlag GmbH & Co. KGaA, Weinheim

of a mobile Al friction layer and fixed poly(tetrafluoroethylene) (PTFE) friction layer with aluminum (Al) electrode stuck on the back side. The relative displacement between the two friction layers is defined with a parameter *D*, as marked in Figure 1a. The ion-gel capacitor is connected in series with the TENG operated in contact–separation mode. When two friction layers in TENG contact with each other ($D = 0$, the initial state (I)), opposite charges are induced at the contact interface due to electrostatic induction. At this stage, the negative and positive charges are balanced and no charges are transferred to the two electrodes of the ion gel capacitor. Thus, the ions distribute uniformly in electrolyte, in which there is no triboelectric potential drop (V_{TENG}) or induced electric field (E) (bottom panel in Figure 1a). When the two friction layers separate at a certain distance (II), the induced opposite charges cannot be fully balanced and partially transfer to the two electrodes of the ion gel capacitor, which make the two electrodes negatively and positively charged, respectively. When the two friction layers further separate (III–VI), more induced charges transfer to the electrodes of the capacitor and attract more compensated ions. The relevant triboelectric potential drop across the EDLs is increased and leads to higher electric field at the interfaces. The dynamic formation process of EDLs in ion gel under a constant triboelectric potential (constant separation distance at *D*) is explained in Figure S1 (Supporting Information).

To better understand the working mechanism of the triboiontronic transistor, the equivalent electrostatic charges transferred from TENG to the gate electrode under a separation–contact–separation cycle process were quantitatively analyzed by an electrometer (Keithley 6514 system). The separation–contact–separation process of two friction layers was considered as a triboelectrification period. With the separation distance (*D*) of TENG varied at a step of 20 μm in one period (separation–contact–separation), the amount of transferred charges was firstly increased from 0 to 6.3 nC (separation process), then decreased to –9.7 nC (contact process) and finally recovered to 0 nC (separation process), varying steadily and synchronously with *D*. The variation of the transferred charges exhibited a sinusoidal manner in one separation–contact–separation cycle (Figure 1b). When the separation distance of TENG decreased by 20 μm in one step, about 2 nC negative charges transferred from TENG to side gate electrode, corresponding to the formation of EDLs. When the separation distance of TENG increased by one step, about 2 nC negative charges transferred from side gate electrode back to TENG electrode, corresponding to the recovery of EDLs. Therefore, the transferred charges contribute a positive (or negative) gate voltage to the transistor. The detailed measurements and analysis are shown in Figure S2 (Supporting Information). Notably, stable transferred charges are critical to insure the triboiontronic transistor to operate steadily and synchronously, which is attributed to the good electronic insulating property of ion liquid after gelation and the encapsulation of the source–drain electrodes with poly(methyl methacrylate) (PMMA) (this will be discussed in details below).

The effective capacitance (C_{eff}) of the utilized ion gel was characterized by applying a small AC voltage at different frequencies to a typical metal–insulator–metal (MIM) structure using an electrochemical workstation. The MIM structure was constructed by patterning ion gel across the evaporated Au electrodes. Figure 1c shows the C_{eff} of the ion gel versus the frequency (f) of the applied AC voltage. The effective capacitance was over 10 μF cm^{-2} at a low frequency of 100 Hz and still higher than 1 μF cm^{-2} at 5000 Hz, which was estimated from the Nyquist plot using the out-of-phase impedance ($Z'' = 1/2\pi fC_{eff}$) (Figure S3a, Supporting Information). Relatively high capacitance indicated the gelation polymer network did not inhibit the migration speed of the ions (i.e., ionic mobility). In order to further elaborate the ion migration and EDL formation process during the triboelectric potential gating, phase angle and equivalent circuit diagram analysis were further discussed in Figure S3b,c (Supporting Information).

The dielectric properties of the ion gel were characterized by *C*–*V* measurement with a MIS structure. The specific capacitance of the device increases with the gate voltage increasing from –0.6 to 0.6 V (Figure 1d), which is attributed to the accumulation of electrons at the ion-gel/MoS_2 channel interface under positive gate bias. The maximum capacitance reached 5.9 μF cm^{-2}, which was much larger than the capacitances of traditional dielectric layers (e.g., 11.5 nF cm^{-2} for 300 nm SiO_2 dielectric). According to the existence of ions migration during the triboelectric potential gating process, ion-gel/semiconductor interface properties were critical to the device operation. Within the electrochemical potential windows, the ions in the ion gel interacted with MoS_2 surface through van der Waals forces or electrostatic interaction without chemical reactions. The inert chemical reactivity of the ionic liquid prevented the chemical bonding at the EDL interface. The small hysteresis in the *C*–*V* curve further demonstrated the gate bias mainly contributed to the charge accumulation in ion gel instead of inducing electrochemical reactions.

The schematic illustration of the triboelectric potential driven ion-gel-gated MoS_2 FET is shown in **Figure 2**a. The nanoflakes of MoS_2 were directly grown on silicon wafer (Si/SiO_2, 300 nm) by chemical vapor deposition (CVD). The source–drain electrodes and the coplanar side gate electrode (10 nm/50 nm) were simultaneously defined by standard e-beam lithography (EBL) and thermal deposition. Then the source–drain electrodes were covered with a layer of PMMA (200 nm) through a second EBL process. Finally, the ion gel dielectric layer was patterned across the MoS_2 channel and a portion of the side gate electrode. The TENG (Al/PTFE-Al structure in contact–separation mode) was connected to the side gate of MoS_2 transistor in series to insure the triboelectric potential was capacitively coupled to MoS_2 channel through ion gel. The optical photograph of the as-synthesized monolayer MoS_2 flakes is displayed in Figure S4a (Supporting Information). The Raman spectroscopy and photoluminescence (PL) spectra of MoS_2 with the excitation wavelength of 532 nm at different intensities are shown in Figure S4b,c (Supporting Information). The wavenumber difference between in-plane vibration modes E_{2g} and out-of-plane vibration modes A_{1g} was about 20 cm^{-1}. The monolayer MoS_2 displayed a strong PL peak at 1.8 eV, originating from its bandgap. Figure 2b displays the typical output characteristics (I_D–V_D, where I_D is the drain current and V_D is the drain voltage) of an ion-gel-gated MoS_2 transistor at different gate voltages (V_{GS}). The drain current increased from 12.9 pA to 5.2 μA with the gate voltage increased from 0 to 0.6 V at a V_D of 0.5 V. The I_D–V_D characteristics showed

© 2018 WILEY-VCH Verlag GmbH & Co. KGaA, Weinheim

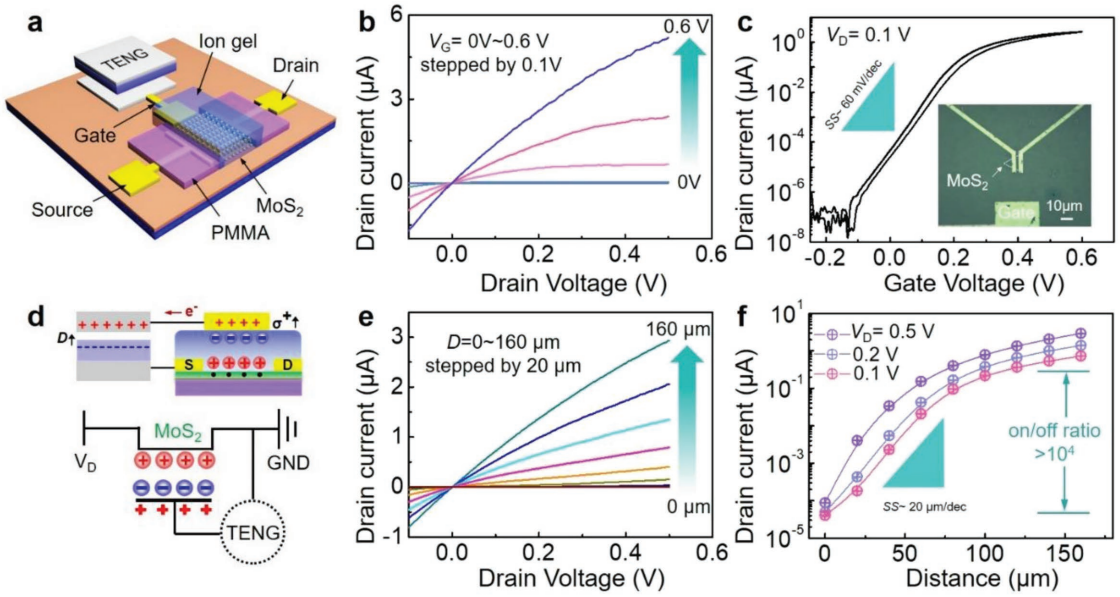

Figure 2. a) Schematic illustration of the triboiontronic transistor of MoS_2. b) Typical output characteristics of the ion-gel-gated MoS_2 transistor. c) Typical transfer characteristics of the ion-gel-gated MoS_2 transistor. Inset is the optical photograph of the device. d) The working state and circuit diagram of triboiontronic MoS_2 transistor in E-mode. e) The output characteristics and f) transfer characteristics of the E-mode triboiontronic MoS_2 transistor, with current on/off ratio over 10^4.

an increment trend of channel conductance with the increase of V_G. The I_D showed a linear dependence in the low V_D region and a saturated trend at high V_D. In order to obtain higher performance of the device, output characteristics of the different ion-gel-gated MoS_2 transistors with larger sweep range have also been measured, as shown in Figure S5 (Supporting Information). Figure 2c displays the transfer characteristics (I_D–V_G) in logarithmic scale of the ion-gel-gated MoS_2 transistor. The drain current was measured with V_G sweeping from –0.25 to 0.6 V. A small V_D of 0.1 V was applied to ensure the transistor operated in the linear region. The MoS_2 transistor showed a high current on/off ratio at $\approx 10^7$ with small hysteresis (consistent with the C–V curves in Figure 1d), indicating no electrochemical reactions or irreversible chemical bonding occurred at the EDL interface. Without hysteresis, the performance of transistor was more predictable. An ultralow cut-off current (0.1 pA) was obtained at small pinch-off voltage (V_G = –0.1 V) due to the ultrahigh capacitance of the ion-gel gate dielectric. The transistor showed a relatively small threshold voltage (V_T) at 0.2 V and a reasonable transconductance (g_m) of 0.6 μS at the linear region (Figure S6, Supporting Information). The field-effect electron mobility (μ) of the ion-gel-gated transistor was extracted to be 9 $cm^2\ V^{-1}\ s^{-1}$. The electrical performances of ion-gel-gated MoS_2 transistor with two different channel thicknesses were measured as shown in Figure S7 (Supporting Information). Different thicknesses led to different performances. Higher current on/off ratio was observed for thin MoS_2 flake samples. The "ON" state conductivity was almost unchanged due to the electrons accumulation, while the "OFF" state conductivity decreased dramatically. This tendency can be explained by the decreasing of the transport contributed by the inside layers of the channel beneath the surface.[39]

In the triboiontronic device, the triboelectric potential determined by the displacement of TENG replaced the applied gate voltage to drive the MoS_2 FET. A representative operation state of the triboiontronic FET and the equivalent circuit diagram are shown in Figure 2d. When the two friction layers (PTFE and Al) separated with a distance (D), the induced positive charges on Al electrode transferred to the gate electrode, which attracted anions to the gate/ion-gel interface to form an EDL. Meanwhile, the cations were repelled to the ion-gel/MoS_2 interface and accumulated the electrons in MoS_2 channel, inducing another EDL. This process was equivalent to applying a positive gate voltage. The triboelectric potential (V_{TENG}), which is equivalent to the gate voltage of the triboiontronic transistor, can be derived through the electrostatic balance condition (expresses as $V_G = V_{TENG} = Q/C_{eff}$, where Q is the induced charge quantity in the gate electrode and C_{eff} is the MIS effective capacitance.[11]). The triboelectrification induced EDL (T-EDL) acts as a nanogap capacitor and possesses high capacitance values to create large electric fields at the interface, which is capable of accumulating much higher electrons density in MoS_2 channel compared with traditional oxide or polymer gate dielectric. Figure 2e displays the output characteristics of the triboiontronic MoS_2 transistor under different displacements. The drain current increased with the increased displacements and exhibited a similar trend with Figure 2b, indicating the triboelectric potential originated from the displacement of TENG is effective to gate the MoS_2 FET. The detailed working mechanism of triboiontronic FET is discussed in Figure S8 (Supporting Information). Figure 2f displays the transfer characteristics (I_D – D) in logarithmic scale of the triboiontronic MoS_2 transistor, which are extracted from I_D – V_D characteristics. The drain current increased from 88.5 pA to 2.9 μA when D changed from 0 to 160 μm at a V_D of 0.5 V. The displacement of 160 μm was quantified as an

© 2018 WILEY-VCH Verlag GmbH & Co. KGaA, Weinheim

equivalent gate voltage of 0.35 V. The achieved current on/off ratio was only ≈10^4 at V_D = 0.1 V, which was much smaller than that achieved by applying gate voltage. This was attributing to that the triboiontronic transistor only worked in the enhancement mode (E-mode) when the displacement gradually increased (i.e., only positive triboelectric potential was coupled to the device).

The essence of triboiontronic FET is a series connection of TENG and ion-gel-gated transistor through capacitive coupling. The triboelectric potential originates from the electrostatic induction charges. Generally, TENG displacement starts from full contact situation. The induced electrostatic charges coupled to FET are either positive (or negative, through reverse connection) due to the only option of displacement in separation mode. As shown in Figure 2f, I_D of the triboiontronic FET is only cutoff to be ≈10^{-5} μA due to the transistor working in E-mode. To achieve high performance triboiontronic MoS_2 FET, it is necessary to deplete the remained electrons in the channel by triboelectric potential gating to further decrease the off-current. The depletion mode (D-mode) of triboiontronic transistor was introduced by presetting the initial separation distance between two friction layers of TENG. At the initial separation distance, the induced charges on TENG were neutralized by grounding one of the electrodes or connecting the two electrodes. Thus, there was no triboelectric potential drop on the transistor. When the distance decreased, the negative charges were induced and transferred to the gate, leading to the depletion of charge carrier in the channel. As shown in **Figure 3**b, the mobile Al electrode was connected to the gate electrode. In the separation state, unbalanced positive charges induced on the Al electrode would transfer to the gate electrode, equivalent to a positive gate voltage. The presetting process was conducted through grounding the mobile Al electrode in a preseparated TENG (with an initial distance D_0, 200 μm) to release the induced positive charges and get a zero triboelectric potential at the separation state (i.e., D_0). Thus, further separation would reinduce positive charges on the mobile Al electrode and realize a positive gate voltage coupled to MoS_2 channel. In contrast, contact process between Al and PTFE would lead to an equivalent negative gate voltage, attributing to that the positive charges transfer out from gate to Al electrode to balance the negative charges induced in PTFE.

The operation mechanisms of the triboiontronic transistors working in flat band, E-mode and D-mode is described below,

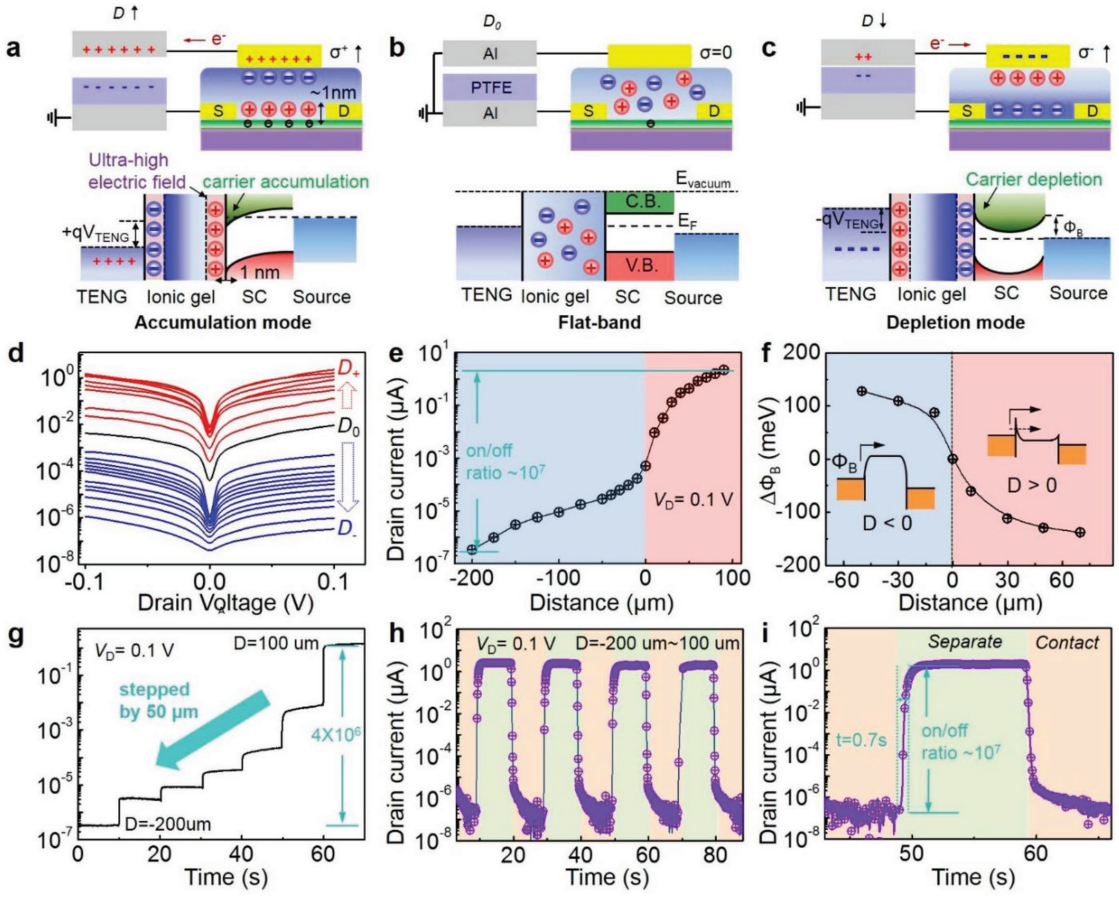

Figure 3. a–c) The working mechanism of triboiontronic transistor after presetting the initial separation distance. Bottom panels are energy band diagrams for three operation states of triboiontronic transistor: accumulation (enhancement), flat-band, and depletion modes. d) The output characteristics of the triboiontronic MoS_2 transistor. e) The transfer characteristics of the triboiontronic MoS_2 transistor with on/off ratio over 10^7. f) The Schottky barrier height variation versus D. Inset is the corresponding energy band diagrams. g) The real-time test with the distance decreased from 100 to −200 μm. h) Dynamic test of triboiontronic MoS_2. i) The enlarged view of one period in Figure 3h.

© 2018 WILEY-VCH Verlag GmbH & Co. KGaA, Weinheim

respectively. The bottom panel in Figure 3b shows the flat band state of the triboiontronic transistor. As there is no charge transfer from TENG to the gate electrode in this state, the ions randomly distribute in the ion gel, imposing no effect on the Fermi level shift of MoS_2. When the displacement D gradually increases ($D > D_0$, Figure 3a), more unneutralized positive charges are induced on Al electrode and transferred to side gate electrode. The positive charge density (σ^+) on side gate electrode increases simultaneously, leading to an equivalent positive gate voltage coupled to the MoS_2 channel. The positive triboelectric potential attracts the anions to migrate toward gate/ion-gel interface and repels cations to the ion-gel/MoS_2 interface. Thus, high electrons density is accumulated in MoS_2 channel due to the ultrahigh electric field, which bends the energy band downward and decreases the energy barrier between source electrode and MoS_2 channel. Electrons are easier to inject into the conduction band across the decreased energy barrier, resulting in increased output current. For this situation, the device works in E-mode. On the other hand, when the displacement D gradually decreases ($D < D_0$, Figure 3c), more positive charges are attracted from gate to Al electrode to neutralize with the induced electrons in PTFE. The left electrons transfer to side gate electrode simultaneously, which causes the negative charge density (σ^-) on side gate electrode increased continuously (equivalent to increased negative gate voltages). The negative triboelectric potential forces the cations to migrate toward gate/ion-gel interface and repels anions to the ion-gel/MoS_2 interface. Hence, the remained electrons in MoS_2 channel at the flat band state are efficiently depleted, which bends the energy band upwards and increases the energy barrier between source electrode and MoS_2 channel. The electrons are prevented from injection into the conduction band of the semiconductor, causing great decrement of the off-state output current (i.e., the depletion mode). Thus, through changing the displacement of TENG, the carrier density in semiconductor channel can be electrostatically controlled. Both accumulation and depletion modes were achieved in one triboiontronic device through presetting the initial separation distance. The prompt motion of cations and the anions creates a strong accumulation of space charges at the gate–electrolyte and semiconductor–electrolyte interfaces in the form of triboelectric potential-induced EDLs. At the interfaces, the triboelectric potential-induced EDLs can act as a nanogap (≈1 nm) capacitor, which process high capacitance and create large electric fields. Figure 3d displays the output characteristics of the triboiontronic MoS_2 transistor working in both D-mode and E-mode. The output currents showed stepped increments (decrements) with increased (decreased) displacements (stepped by 10 μm), demonstrating good electrostatic control capacities of T-EDLs in both working modes. Figure 3e displays the corresponding transfer characteristics ($I_D - D$) of the triboiontronic MoS_2 transistor, extracted from $I_D - V_D$ characteristics in Figure 3d. The depletion working mode greatly decreased the off-state current to 0.3 pA at $V_D = 0.1$ V with a TENG displacement at −200 μm. The achieved current on/off ratio exceeded 10^7, comparable with counterpart under applied gate voltage.

To further analyze the transport properties of the obtained triboiontronic device, a thermionic-emission theory was employed to model the charge carriers transport behavior. According to this theory, the saturation current (I_{sat}) flowing through a Schottky barrier is described as: $I_{sat} = AA^* T^{3/2} \exp\left(-\frac{q\Phi_B}{k_B T}\right)$, where A is the contact area, $A^*$is the Richardson constant, Φ_B is the height of Schottky barrier between the source electrode and MoS_2 channel, T is temperature, κ_B is the Bolzmann constant, q is the elementary charge.[40,41] The Schottky barrier height variation ($\Delta\Phi_B$) can be derived from the output characteristics according to $\ln(I_t/I_0) = -q\Delta\Phi_B/kT$, where I_t and I_0 are the drain currents measured at a fixed V_D with and without triboelectric potential gating, respectively.[42] As shown in Figure 3f, with the variation of TENG displacement, the Schottky barrier at the source/channel contact can be greatly modulated (≈265 meV, $T = 300$ K). When $D < 0$, negative triboelectric potential depleted electrons in MoS_2 channel and increased the Schottky barrier height. In this case, I_D was mainly determined by thermionic emission current ($I_{thermionic}$). When $D > 0$, positive triboelectric potential accumulated the electrons in MoS_2, The Schottky barrier height was decreased and its width was shortened. Then, the thermally assisted tunneling current ($I_{tunneling}$) appeared and contributed to I_D together with $I_{thermionic}$. To accurately calculate the Schottky barrier height, temperature-dependent studies should be carried out in further study.

The real time test of the triboiontronic transistor with the large range of displacement (from 100 to −200 μm, stepped by 50 μm) was also performed (Figure 3g). The output current decreased from 1.4 μA to 0.3 pA with displacement from 100 to −200 μm. At each step of TENG displacement, the I_D exhibited corresponding variations and maintained at stable values. Notably, the maintainable output currents induced by triboelectrostatic charges was attributed to the low leakage current (I_G) and excellent electronic insulating properties of ion gel gate dielectrics. To obtain the low leakage current, PMMA encapsulation of source–drain electrodes was critical to prevent the triboelectric charges (induced by triboelectrification and electrostatic induction) flowing from gate to source electrode and reduce I_G to sub-pA level (Figure S9, Supporting Information). The solidification of ion gel (i.e., restricting ion liquid molecular in a polymer network to get a solid-like composite) also contributed to reduce the leakage current. The excellent cycling properties of triboiontronic transistor with TENG displacement at 300 μm is shown in Figure 3h. Both the on/off-state currents were maintained stable. A remarkable current on/off ratio exceeding 10^7 was achieved. Relatively short response time of 0.7 s was extracted from one cycle of contact–separation test (Figure 3h). According to the encapsulation of the electrode by PMMA, the gate leakage current had been decreased to ≈pA level, which ensured the long term stability of the triboiontronic transistor. The triboelectric charges might gradually decrease according to the neutralization by the opposite charges in the air. This problem could be fully resolved by recalibrating the triboelectric potential through resetting the initial contact distance.

The figure-of-merits of triboiontronic transistors including tribotronic transconductance (g_t), threshold value (D_T), and subthreshold swing (SS_t) are investigated in details in Figure S6 (Supporting Information). The g_t, D_T, and SS_t were characterized to be 43.5 nA μm^{-1}, 80 μm, and 20 μm dec^{-1}, respectively. All of

© 2018 WILEY-VCH Verlag GmbH & Co. KGaA, Weinheim

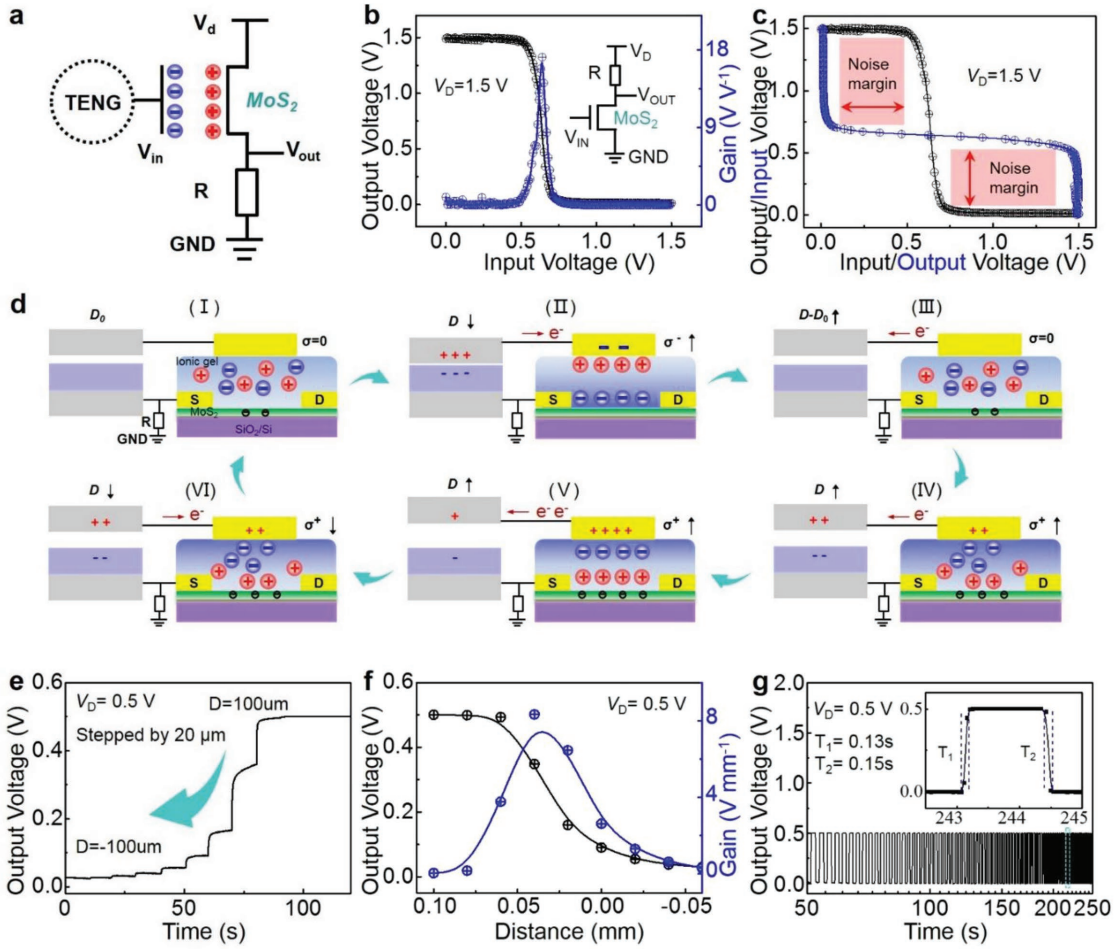

Figure 4. a) Circuit diagram of triboiontronic logic device. b) Typical voltage transfer characteristics of ion-gel-gated MoS_2 inverter and corresponding gain value. c) The noise margin of the inverter. d) The working principle and the operation process of the triboiontronic MoS_2 inverter. e) The real-time testing the triboiontronic MoS_2 inverter with the distance decreased from 100 to −100 μm. f) The voltage transfer characteristics of the triboiontronic MoS_2 logic inverter. g) Cycle stability test of the triboiontronic MoS_2 inverter (100 cycles). Inset shows the response time of increment (T_1) and decrement (T_2) is 0.13 and 0.15 s, respectively.

them were greatly improved compared with the counterparts in tribotronic MoS_2 FET with SiO_2 dielectric (e.g., 0.18 μA mm^{-1}, 13 mm, and 4.6 mm dec^{-1}, respectively).[14] All the results above demonstrated a high performance triboiontronic MoS_2 FET due to the highly efficient gating properties from T-EDLs.

After achieving the stable triboiontronic transistors in high performance, corresponding logic devices coupled with TENG were demonstrated by matching a resistor (100 MΩ) with the triboiontronic MoS_2 transistor (**Figure 4**a). Typical voltage transfer characteristics of the counterpart inverter with applied gate voltage are shown in Figure 4b. A resistor is connected in series with MoS_2 transistor (inset circuit diagram). Under the superposition effect of an applied V_D at 0.5 V, the voltage drop on the series resistor varied according to the resistance change of the MoS_2 transistor, leading to an inverted signal between the input (V_{IN}) and output voltage (V_{OUT}). To characterize the sharp transition properties, the voltage gain (G_V, expressed as $G_V = -dV_{OUT}/dV_{IN}$) was calculated to reach the maximum value of 17 at the logic switching point (0.64 V), qualified to drive back-end gates. The logic separation was almost ideally equal to V_D (1.5 V) and the noise margin was higher than 30% of V_D (Figure 4c) for the tolerance of the inverter to intrinsic or extrinsic noise. The ion-gel-gated MoS_2 inverter showed excellent inverting performance, analogous rail-to-rail separation and high noise margin, offering a good foundation to fabricate complicated triboiontronic logic devices with good performance.

Figure 4c shows the working principle and the operation process of the triboiontronic logic inverter. At the initial state (I, D_0), the triboelectric potential was preset to be zero, no charges were induced on the gate electrode (σ = 0). At the second state (II, D decreasing), the electrons transferred from top Al electrode to gate electrode, which produced a negative triboelectric potential and depleted the electrons in the channel. The MoS_2 transistor was at high resistance state and the output voltage was at low level ("0"). From the third to fifth state (III–V), with D gradually increased, the electrons transferred from gate electrode to top Al electrode to neutralize the induced positive charges, leading to the triboelectric potential coupled to MoS_2 transistor switching from negative value to positive value.

© 2018 WILEY-VCH Verlag GmbH & Co. KGaA, Weinheim

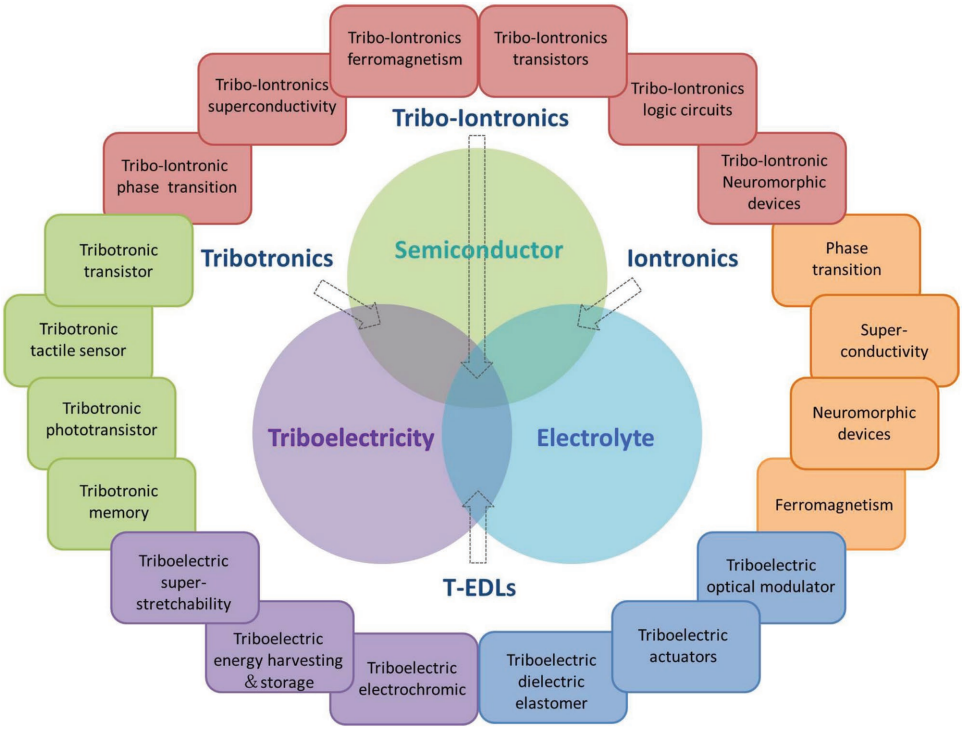

Figure 5. Perspectives on triboiontronic transistor and related fields.

Thus, the electrons in the channel were accumulated. The transistor turned to low-resistance state and the output voltage changed from low level ("0") to high level ("1"). At the sixth state (VI) (D decreasing to D_0), the electrons transferred from top Al electrode back to gate electrode, the triboelectric potential decreased and returned to zero. The output voltage of the device was mainly extracted from state III to state V, with D varied between 100 and –100 µm. Figure 4e shows the dynamic test of the triboiontronic inverter logic device. With the displacement changing from 100 to –100 µm stepped by 20 µm, the output voltage changed from 0.5 V ("1" state) to 0.02 V ("0" state), indicating a large logic separation of 0.498 V. Figure 4f shows the voltage transfer characteristics of the triboiontronic logic inverter extracted from Figure 4e, consistent with the working principle discussed above (state (III–V)). The sharp transition between the two logic states can be characterized by the gain (G_D) versus distance D, expressed by $G_D = -\mathrm{d}V_{OUT}/\mathrm{d}D$. The G_D reached the maximum value of 8.3 V mm^{-1} at the logic switching point. To demonstrate the robustness of the triboiontronic logic device, over 100 cycle tests had been performed with stable logic separations, as shown in Figure 4g. The inset displaced one cycle test, demonstrating a fast response time with rise time T_1 = 0.13 s and fall time T_2 = 0.15 s. The stable output performance in Figure 4g can also reflect excellent long term stability of MoS_2 based transistor. The corresponding current of the triboiontronic inverter is shown in Figure S10 (Supporting Information). The average static power consumption (P_S) was defined as $P_S = V_D \cdot (I_{D\ (Vout\ =\ 0\ V)} + I_{D(Vout\ =\ 0.5\ V)})/2$, and the triboiontronic inverter showed a small average static power consumption of 0.025 nW at V_D = 0.5 V.

Based on the results above, electronic transport behaviors of MoS_2 FET and logic devices are efficiently modulated by mechanically triggered ions migration and arrangement. **Figure 5** shows the perspective of triboiontronics based on coupling among triboelectricity, semiconductor devices, and electrolyte modulation. As the building block of ion-controlled electronics, EDL–FET promises a highly efficient control of charge carrier density in low voltage, driving great development of high performance printable organic electronics, artificial neuromorphic devices, phase transition induced superconductivity, and magnetic anisotropy, etc.[24] The triboelectricity induced by TENG has been correlating with electrolytes (or ion-contained materials).[43,44] On one hand, batteries, supercapacitors,[45] dye-sensitize solar cells, electrochromic devices, and hydrogels have been extensively studied for triboelectric energy package (integrated energy harvesting and storage),[46] hybrid energy harvesting,[45,47] smart sensing, and superstretchability.[43] On the other hand, ion-contained elastomers driven by TENGs have recently been developed for optical grating and mechanical actuation. When the triboelectricity induced by TENG couples with semiconductor devices, the emerging tribotronics introduce the logic function of switching or computation, covering tribotronic transistor, derived tribotronic memory, and logic devices.[12] For further and more efficient coupling of triboelectric potential and electronic properties, three-term coupling (triboelectricity, semiconductor, and electrolyte) is of great significance to utilize EDL modulation as the bridge, pushing forward an interdisciplinary concept of triboiontronics. The formation of the electrical double layers (i.e., high-density carrier accumulation, high electric fields, and large capacitances) is triggered by mechanical interaction in triboiontronic transistor. This method is ready to applicable to different types of semiconductor materials, such as inorganic semiconductors, organic small molecules, polymer semiconductor, oxide

© 2018 WILEY-VCH Verlag GmbH & Co. KGaA, Weinheim

semiconductors, phase transition materials, superconductive materials, etc. Based on this, the triboiontronic transistor is able to be utilized as a platform for mechanical instruction triggered phase transition, superconductivity, ferromagnetism, thermoelectric devices and high performance E-skin. Take advantage of ions migration and arrangement triggered by mechanical interaction, triboiontronic transistor is ready to deliver triboiontronic superconductivity, triboiontronic ferromagnetism, triboiontronic E-skin, triboiontronic afferent neuron, etc.

In summary, a triboiontronic transistor was proposed for the first time, which bridged the triboelectric potential modulation and ion-controlled semiconductor devices. Instead of applying gate voltage, the triboelectric potential was used to control the transport behavior of the device through the T-EDLs, which formed at the interface of ion-gel/semiconductor. Taking advantage of T-EDLs, which included high density carrier accumulation, high electric field and large capacitance, a high performance triboiontronic MoS_2 transistor had been demonstrated with high current on/off ratio, low threshold value, and steep switch properties. The triboiontronic logic inverter also exhibited a desirable gain of (8.3 V mm^{-1}), low power consumption, and high stability. This work presents a low-power-consuming, highly efficient and a universal approach to modulate ion-controlled semiconductor devices and logic circuits based on 2D materials through external mechanical instructions. The proposed triboiontronics, in three-term coupling of triboelectricity, semiconductor, and electrolyte, are ready to deliver unprecedented physics characteristics interacted with mechanical motions.

Experimental Section

Materials Preparation: MoS_2 was grown on a Si wafer (with 300 nm thermally grown SiO_2) by CVD. Sulfur pieces (Alfa Aesar 99.9%) and molybdenum trioxide power (MoO_3) (Alfa Aesar 99.999%) were used as precursors. During the growth process, the MoO_3 power in the quartz tube was heated to 850 °C at a rate of 30 °C min^{-1}, and the sulfur pieces were heated to 150 °C at the same speed. 50 sccm Argon was used as carrier gas of the precursors and the pressure of the system was kept at 1 kPa during the synthesis process. To make sure the monolayer MoS_2 growth without defects and multilayer deposition, 4 sccm O_2 was bubbled into the tube during the growth process. The whole growth time lasted for 3 min. The tube was quickly cooled down to room temperature after the synthesis process.

Device Fabrication: After the preparation of MoS_2 on the Si wafer, the source–drain electrodes and the coplanar side gate electrode were simultaneously defined by standard EBL and thermal evaporation deposition of Cr/Au (10 nm/40 nm, respectively). To minimize the damage of the MoS_2 surface, the deposition rate was fixed at 1 Å s^{-1} for Cr and 2 Å s^{-1} for Au. Then the source–drain electrodes were covered with a layer of PMMA with 200 nm through a second EBL process. Finally, a layer of ion gel was patterned on the channel and partial side gate electrodes of the transistor. TENG composed of an Al–PTFE–Al structure was connected to the side gate electrode of MoS_2 FET. In order to fabricate the ion gel dielectrics, an ion gel ink comprising of 1-ethyl-3-methylimidazolium bis(trifluoromethylsulfonyl) imide (EMIM:TFSI) ionic liquid, poly(ethylene glycol) diacrylate (PEGDA) monomer, and 2-hydroxy-2-methylpropiophenone (HOMPP) photoinitiator (weight ratio of 90:8:2) was drop-casted onto the MoS_2 transistor. A patterned photomask was placed onto the ion gel, and the device was exposed to ultraviolet light (UV) (365 nm, 100 mW cm^{-2}) for 10 s. After that, the region exposed to UV light was photo-crosslinked, while the unexposed region could be removed by deionized water.

Performance Characterization: The electrical characterizations of the triboiontronic transistors and logic devices were conducted with a semiconductor parameter analyzer (Agilent B1500A) in a probe station under ambient environment. The displacements of TENGs were controlled by a linear motor. The output properties of TENG were measured by Keithley 6514 system electrometer. The capacitive and impedance analysis was conducted by applying a small AC voltage at different frequencies using an electrochemical workstation. During the test, the device and the TENG should be well screened to avoid the electric surge from breaking down the triboiontronic transistor by the surrounding electrostatic charges.

Supporting Information

Supporting Information is available from the Wiley Online Library or from the author.

Acknowledgements

G.G., J.Y., and X.Y. contributed equally to this work. This work was financially supported by the National Key Research and Development Program of China (2016YFA0202703, 2016YFA0202704), the National Natural Science Foundation of China (51605034, 51711540300, 51475099), the "Hundred Talents Program" of the Chinese Academy of Science, Beijing Natural Science Foundation (4184111) and state key laboratory of precision measuring technology and instruments (Tianjin University).

Conflict of Interest

The authors declare no conflict of interest.

Keywords

electrical double layers, ion-gel-gated MoS_2 transistors, triboelectric nanogenerators, triboiontronic logic inverters, triboiontronic transistors

Received: October 25, 2018
Revised: December 11, 2018
Published online: December 27, 2018

[1] F. R. Fan, L. Lin, G. Zhu, W. Z. Wu, R. Zhang, Z. L. Wang, *Nano Lett.* **2012**, *12*, 3109.
[2] Z. L. Wang, *Nature* **2017**, *542*, 159.
[3] Z. L. Wang, *ACS Nano* **2013**, *7*, 9533.
[4] H. Guo, X. Pu, J. Chen, Y. Meng, M.-H. Yeh, G. Liu, Q. Tang, B. Chen, D. Liu, S. Qi, C. Wu, C. Hu, J. Wang, Z. L. Wang, *Sci. Rob.* **2018**, *3*, eaat2516.
[5] X. D. Wang, Y. F. Zhang, X. J. Zhang, Z. H. Huo, X. Y. Li, M. L. Que, Z. C. Peng, H. Wang, C. F. Pan, *Adv. Mater.* **2018**, *30*, 1706738.
[6] X. J. Pu, H. Y. Guo, J. Chen, X. Wang, Y. Xi, C. G. Hu, Z. L. Wang, *Sci. Adv.* **2017**, *3*, e1700674.
[7] A. Y. Li, Y. L. Zi, H. Y. Guo, Z. L. Wang, F. M. Fernandez, *Nat. Nanotechnol.* **2017**, *12*, 481.
[8] J. Cheng, W. B. Ding, Y. L. Zi, Y. J. Lu, L. H. Ji, F. Liu, C. S. Wu, Z. L. Wang, *Nat. Commun.* **2018**, *9*, 3733.
[9] A. Ahmed, I. Hassan, T. Ibn-Mohammed, H. Mostafa, I. M. Reaney, L. S. C. Koh, J. Zu, Z. L. Wang, *Energy Environ. Sci.* **2017**, *10*, 653.

 © 2018 WILEY-VCH Verlag GmbH & Co. KGaA, Weinheim

[10] P. Song, S. Kuang, N. Panwar, G. Yang, D. J. H. Tng, S. C. Tjin, W. J. Ng, M. B. A. Majid, G. Zhu, K.-T. Yong, Z. L. Wang, *Adv. Mater.* **2017**, *29*, 1605668.
[11] C. Zhang, W. Tang, L. M. Zhang, C. B. Han, Z. L. Wang, *ACS Nano* **2014**, *8*, 8702.
[12] C. Zhang, Z. L. Wang, *Nano Today* **2016**, *11*, 521.
[13] Y. Liu, S. M. Niu, Z. L. Wang, *Adv. Electron. Mater.* **2015**, *1*, 1500124.
[14] G. Y. Gao, B. S. Wan, X. Q. Liu, Q. J. Sun, X. N. Yang, L. F. Wang, C. F. Pan, Z. L. Wang, *Adv. Mater.* **2018**, *30*, 1705088.
[15] F. Xue, L. B. Chen, L. F. Wang, Y. K. Pang, J. Chen, C. Zhang, Z. L. Wang, *Adv. Funct. Mater.* **2016**, *26*, 2104.
[16] Z. W. Yang, Y. Pang, L. Zhang, C. Lu, J. Chen, T. Zhou, C. Zhang, Z. L. Wang, *ACS Nano* **2016**, *10*, 10912.
[17] Y. K. Pang, F. Xue, L. F. Wang, J. Chen, J. J. Luo, T. Jiang, C. Zhang, Z. L. Wang, *Adv. Sci.* **2016**, *3*, 1500419.
[18] J. Li, C. Zhang, L. Duan, L. M. Zhang, L. D. Wang, G. F. Dong, Z. L. Wang, *Adv. Mater.* **2016**, *28*, 106.
[19] Y. F. Meng, J. Q. Zhao, X. X. Yan, C. L. Zhao, S. S. Qin, J. H. Cho, C. Zhang, Q. J. Sun, Z. L. Wang, *ACS Nano* **2018**, *12*, 9381.
[20] J. H. Cho, J. Lee, Y. Xia, B. Kim, Y. He, M. J. Renn, T. P. Lodge, C. D. Frisbie, *Nat. Mater.* **2008**, *7*, 900.
[21] M. N. Fujii, Y. Ishikawa, K. Miwa, H. Okada, Y. Uraoka, S. Ono, *Sci. Rep.* **2016**, *5*, 18168.
[22] K. H. Lee, M. S. Kang, S. Zhang, Y. Gu, T. P. Lodge, C. D. Frisbie, *Adv. Mater.* **2012**, *24*, 4457.
[23] J. Lee, M. J. Panzer, Y. Y. He, T. P. Lodge, C. D. Frisbie, *J. Am. Chem. Soc.* **2007**, *129*, 4532.
[24] S. Z. Bisri, S. Shimizu, M. Nakano, Y. Iwasa, *Adv. Mater.* **2017**, *29*, 1607054.
[25] T. Fujimoto, K. Awaga, *Phys. Chem. Chem. Phys.* **2013**, *15*, 8983.
[26] Q. Sun, D. H. Kim, S. S. Park, N. Y. Lee, Y. Zhang, J. H. Lee, K. Cho, J. H. Cho, *Adv. Mater.* **2014**, *26*, 4735.
[27] Q. Sun, W. Seung, B. J. Kim, S. Seo, S. W. Kim, J. H. Cho, *Adv. Mater.* **2015**, *27*, 3411.
[28] Y. Saito, Y. Nakamura, M. S. Bahramy, Y. Kohama, J. T. Ye, Y. Kasahara, Y. Nakagawa, M. Onga, M. Tokunaga, T. Nojima, Y. Yanase, Y. Iwasa, *Nat. Phys.* **2016**, *12*, 144.
[29] Y. Zhang, J. Ye, Y. Matsuhashi, Y. Iwasa, *Nano Lett.* **2012**, *12*, 1136.
[30] Y. Wang, J. Xiao, H. Zhu, Y. Li, Y. Alsaid, K. Y. Fong, Y. Zhou, S. Wang, W. Shi, Y. Wang, A. Zettl, E. J. Reed, X. Zhang, *Nature* **2017**, *550*, 487.
[31] S. Mao, J. B. Chang, H. H. Pu, G. H. Lu, Q. Y. He, H. Zhang, J. H. Chen, *Chem. Soc. Rev.* **2017**, *46*, 6872.
[32] C. J. Wan, G. Chen, Y. M. Fu, M. Wang, N. Matsuhisa, S. W. Pan, L. Pan, H. Yang, Q. Wan, L. Q. Zhu, X. D. Chen, *Adv. Mater.* **2018**, *30*, 1801291.
[33] Y. Kim, A. Chortos, W. Xu, Y. Liu, J. Y. Oh, D. Son, J. Kang, A. M. Foudeh, C. Zhu, Y. Lee, S. Niu, J. Liu, R. Pfattner, Z. Bao, T.-W. Lee, *Science* **2018**, *360*, 998.
[34] J. Zhu, Y. Yang, R. Jia, Z. Liang, W. Zhu, Z. U. Rehman, L. Bao, X. Zhang, Y. Cai, L. Song, R. Huang, *Adv. Mater.* **2018**, *30*, 1800195.
[35] J. S. Ponraj, Z.-Q. Xu, S. C. Dhanabalan, H. Mu, Y. Wang, J. Yuan, P. Li, S. Thakur, M. Ashrafi, K. McCoubrey, Y. Zhang, S. Li, H. Zhang, Q. Bao, *Nanotechnology* **2016**, *27*, 462001.
[36] S. C. Dhanabalan, J. S. Ponraj, H. Zhang, Q. Bao, *Nanoscale* **2016**, *8*, 6410.
[37] B. Radisavljevic, A. Radenovic, J. Brivio, V. Giacometti, A. Kis, *Nat. Nanotechnol.* **2011**, *6*, 147.
[38] K. F. Mak, C. Lee, J. Hone, J. Shan, T. F. Heinz, *Phys. Rev. Lett.* **2010**, *105*, 4.
[39] Y. J. Zhang, J. T. Ye, Y. Matsuhashi, Y. Iwasa, *Nano Lett.* **2012**, *12*, 1136.
[40] A. Allain, J. Kang, K. Banerjee, A. Kis, *Nat. Mater.* **2015**, *14*, 1195.
[41] S. Das, H.-Y. Chen, A. V. Penumatcha, J. Appenzeller, *Nano Lett.* **2013**, *13*, 100.
[42] S. Liu, Q. Liao, S. Lu, Z. Zhang, G. Zhang, Y. Zhang, *Adv. Funct. Mater.* **2016**, *26*, 1347.
[43] X. Pu, M. M. Liu, X. Y. Chen, J. M. Sun, C. H. Du, Y. Zhang, J. Y. Zhai, W. G. Hu, Z. L. Wang, *Sci. Adv.* **2017**, *3*, e1700015.
[44] T. Liu, M. M. Liu, S. Dou, J. M. Sun, Z. F. Cong, C. Y. Jiang, C. H. Du, X. Pu, W. G. Hu, Z. L. Wang, *ACS Nano* **2018**, *12*, 2818.
[45] Z. Wen, M. H. Yeh, H. Y. Guo, J. Wang, Y. L. Zi, W. D. Xu, J. N. Deng, L. Zhu, X. Wang, C. G. Hu, L. P. Zhu, X. H. Sun, Z. L. Wang, *Sci. Adv.* **2016**, *2*, e1600097.
[46] S. S. Qin, Q. Zhang, X. X. Yang, M. M. Liu, Q. J. Sun, Z. L. Wang, *Adv. Energy Mater.* **2018**, *8*, 1800069.
[47] K. Zhao, Y. Yang, X. Liu, Z. L. Wang, *Adv. Energy Mater.* **2017**, *7*, 1700103.

© 2018 WILEY-VCH Verlag GmbH & Co. KGaA, Weinheim